Properties of the Turbulence Associated with Electron-only Magnetic Reconnection in Earth's Magnetosheath

J. E. Stawarz[1] , J. P. Eastwood[1] , T. D. Phan[2], I. L. Gingell[1], M. A. Shay[3] , J. L. Burch[4], R. E. Ergun[5,6], B. L. Giles[7],
D. J. Gershman[7] , O. Le Contel[8], P.-A. Lindqvist[9], C. T. Russell[10] , R. J. Strangeway[10], R. B. Torbert[11], M. R. Argall[11] ,
D. Fischer[12], W. Magnes[12], and L. Franci[13]

[1] Department of Physics, Imperial College London, London, UK; j.stawarz@imperial.ac.uk
[2] Space Science Laboratory, University of California, Berkeley, CA, USA
[3] Department of Physics and Astronomy, University of Delaware, Newark, DE, USA
[4] Southwest Research Institute, San Antonio, TX, USA
[5] Department of Astrophysical and Planetary Sciences, University of Colorado, Boulder, CO, USA
[6] Laboratory for Atmospheric and Space Physics, University of Colorado, Boulder, CO, USA
[7] NASA Goddard Space Flight Center, Greenbelt, MD, USA
[8] Laboratoire de Physique des Plasmas, CNRS, Ecole Polytechnique, Sorbonne Université, Université Paris Sud, Observatoire de Paris, Paris, France
[9] School of Electrical Engineering, KTH Royal Institute of Technology, Stockholm, Sweden
[10] Department of Earth, Planetary, and Space Sciences, University of California, Los Angeles, CA, USA
[11] Department of Physics, University of New Hampshire, Durham, NH, USA
[12] Space Research Institute, Austrian Academy of Sciences, Graz, Austria
[13] School of Physics and Astronomy, Queen Mary University of London, London, UK

Abstract

Turbulent plasmas generate intense current structures, which have long been suggested as magnetic reconnection sites. Recent Magnetospheric Multiscale observations in Earth's magnetosheath revealed a novel form of reconnection where the dynamics only couple to electrons, without ion involvement. It was suggested that such dynamics were driven by magnetosheath turbulence. In this study, the fluctuations are examined to determine the properties of the turbulence and if a signature of reconnection is present in the turbulence statistics. The study reveals statistical properties consistent with plasma turbulence with a correlation length of ∼10 ion inertial lengths. When reconnection is more prevalent, a steepening of the magnetic spectrum occurs at the length scale of the reconnecting current sheets. The statistics of intense currents suggest the prevalence of electron-scale current sheets favorable for electron reconnection. The results support the hypothesis that electron reconnection is driven by turbulence and highlight diagnostics that may provide insight into reconnection in other turbulent plasmas.

Key words: magnetic reconnection – plasmas – turbulence

1. Introduction

Plasma turbulence is ubiquitous across many systems, ranging from planetary magnetospheres to galaxy clusters (e.g., Weygand et al. 2005; Schekochihin et al. 2009; Bruno & Carbone 2013; Cranmer et al. 2015). Earth's magnetosheath is one turbulent plasma that is accessible with high-resolution in situ observations (e.g., Sahraoui et al. 2004; Alexandrova et al. 2008; Huang et al. 2014, 2017; Chasapis et al. 2018). In turbulent systems, nonlinear interactions transfer energy from large to small scales, where energy can be dissipated. The nonlinear interactions tend to form coherent structures with intense localized gradients, known as intermittency, which, in collisional systems, are linked to dissipation. However, in the collisionless plasmas commonly present in space and astrophysical systems, it is not clear which processes dissipate energy from the turbulence (Kiyani et al. 2015 and references therein). Determining the mechanisms responsible for turbulent dissipation is key to solving long-standing problems such as the heating of the solar corona and solar wind.

In collisionless plasmas, turbulent dissipation could occur through stochastic heating (Chandran et al. 2010), resonant interactions, such as Landau damping (Chen et al. 2019), or processes, such as instabilities (Stawarz et al. 2015), occurring at intermittent currents. Another important process, suggested to occur at intermittent current structures, is magnetic reconnection (Matthaeus & Lamkin 1986; Carbone et al.

1990; Servidio et al. 2009; Donato et al. 2012; Franci et al. 2017). Reconnection provides pathways for particle acceleration and subsequent heating, offering a means of energy dissipation (Burch et al. 2016b). Additionally, reconnection generates bulk flows and waves, which feed back into the turbulence, acting as a conversion process between electromagnetic and kinetic energy. The dissipation of waves excited by reconnection may also lead to dissipation.

Observational evidence for turbulence-driven reconnection is difficult to obtain because high-resolution plasma measurements are needed to observe reconnection outflows at small-scale current sheets. Reconnection has been found in turbulent plasmas such as the solar wind (Gosling et al. 2007) and Earth's magnetosheath (Phan et al. 2007). Electromagnetic signatures, suggested to be associated with turbulence-driven reconnection, have been reported at small-scale currents in Earth's magnetosheath with Cluster (Retinò et al. 2007; Sundkvist et al. 2007). Recently, high-resolution plasma measurements from Magnetospheric Multiscale (MMS) have revealed electron jets at small-scale current sheets in the magnetosheath (Yordanova et al. 2016; Vörös et al. 2017; Phan et al. 2018; Wilder et al. 2018) and transition region of Earth's bow shock (Wang et al. 2019; Gingell et al. 2019).

In particular, Phan et al. (2018) made the key observation of oppositely directed electron jets, providing clear evidence of active reconnection. However, these reconnecting current

sheets were not embedded within ion-scale current sheets and did not show evidence of ion jets, indicating the ions may not couple to the events and any heating may only go into electrons. This novel electron-only reconnection was embedded within a qualitatively turbulent interval of the magnetosheath with strong fluctuations and many intense current sheets. Therefore, Phan et al. (2018) suggested that turbulence may be driving the reconnection. However, the properties of the fluctuations were not examined in detail. In this study, we examine the fluctuations within the interval studied by Phan et al. (2018) to determine (i) what the properties of the turbulence that drives electron reconnection are and (ii) if there is a signature of reconnection in the turbulence statistics.

2. Data Set

Data were collected by MMS (Burch et al. 2016a) and include magnetic field (B) measurements from the fluxgate (Russell et al. 2016) and search-coil (Le Contel et al. 2016) magnetometers and particle moments from the Fast Plasma Investigation (FPI; Pollock et al. 2016). A merged fluxgate and search-coil magnetometer data set with a crossover between the instruments from 4 to 7 Hz is used (Argall et al. 2018, in preparation). The current density (j) is obtained from the curlometer technique and FPI moments. In the latter case, $j = qn_e(v_i - v_e)$, where q is the proton charge, n_e is the electron number density, v_i and v_e are the ion and electron velocities, respectively, and v_i is interpolated to the cadence of v_e.

Two intervals of high-resolution (burst) magnetosheath data are analyzed, providing 1/8192 s field measurements and 0.15 s and 0.03 s ion and electron moments, respectively. Figure 1 gives an overview of the magnetosheath data and subsequent bow shock crossing at low resolution, with burst intervals indicated by regions where $|j|$ is plotted. The burst intervals are embedded in an extended region of magnetic fluctuations downstream of Earth's bow shock, which MMS crossed at ∼09:40:00 UTC. A feature at ∼09:25:00 UTC, containing a depletion in $|B|$, enhancement in v_i, and narrowing of the ion energy spectrogram toward those of the solar wind, appears consistent with a partial bow shock encounter.

The burst intervals are trimmed to shorter subintervals, referred to as Interval 1 (09:01:40–09:07:00 UTC) and Interval 2 (09:26:25–09:34:57 UTC). The initial portion of the first burst interval is omitted from Interval 1 due to relatively poor performance of the Taylor hypothesis (see Section 3), and the initial portion of the second burst interval is omitted from Interval 2 to avoid the partial shock encounter. The resulting subintervals are 320 s and 512 s long and contain seven and four potentially reconnecting current sheets, respectively, as identified by Phan et al. (2018). An additional five and two reconnecting current sheets were identified within the omitted segments prior to Intervals 1 and 2, respectively. The intervals each contain over 2.5×10^6 B measurements and over 100 magnetic correlation lengths (λ_c) based on the analysis in Section 4.3. Table 1 summarizes the average plasma parameters for the subintervals, including the background flow speed (v_0), Alfvén speed (v_A), $\delta b/B_0 \equiv \sqrt{\langle|B - \langle B\rangle|^2\rangle}/|\langle B\rangle|$, rms $|j|$ (j_{rms}) from FPI, plasma beta (β_s), gyroradius (ρ_s), and inertial length (d_s), where $\langle...\rangle$ denotes a time average over the interval and $s = i, e$ denotes ions or electrons, respectively.

3. Validity of Taylor Hypothesis

For single-spacecraft measurements, the Taylor hypothesis is commonly used to convert observed timescales to length scales, assuming fluctuations advect past the spacecraft at v_0 faster than the dynamical timescale at the length scale of interest. Using the Taylor hypothesis, spatial lags (ℓ) and wavenumbers (k) are given by $\ell = v_0 \Delta t$ and $k = 2\pi f/v_0$, where Δt is a temporal difference, f is the spacecraft-frame frequency, and the spatial scales are measured in the v_0 direction. In plasmas such as the solar wind, where a unidirectional, super-Alfvénic v_0 is present, the Taylor hypothesis is well founded. For the magnetosheath intervals analyzed here, $v_0 \sim 2v_A$ and the flow directions are ∼47° and 26° relative to B_0 for Intervals 1 and 2, respectively.

Spatial lags can be directly measured using the six spacecraft pairs in the MMS formation. By comparing statistics computed using the Taylor hypothesis and from spacecraft pairs, the Taylor hypothesis can be tested at the scale of the MMS formation (Chen & Boldyrev 2017). In Figure 1(f), single- and multispacecraft estimates of the second-order structure function (S_2) of B, defined as

$$S_2(\ell) = \langle|B(x + \ell) - B(x)|^2\rangle, \qquad (1)$$

are compared as a function of the angle (θ_ℓ) between ℓ and B_0. For the ∼6 km MMS separations, good agreement is found for both intervals, indicating the Taylor hypothesis is valid well below ion scales. Anisotropy with θ_ℓ is not apparent and on average multispacecraft estimates are within 10% of Taylor hypothesis estimates. The super-Alfvénic flows and good agreement between single- and multispacecraft measurements well into the kinetic scales suggest the Taylor hypothesis can be reasonably applied to examine a wide range of scales. In contrast, the omitted segment prior to Interval 1 displays a systematic overestimate of the single-spacecraft estimates relative to the multispacecraft estimates for all six spacecraft pairs, indicating the Taylor hypothesis may not work as well during this interval.

4. Results

4.1. Magnetic Spectra

Omnidirectional magnetic spectra for both intervals with k computed using the Taylor hypothesis are displayed in Figure 2. The spectra exceed the noise floor of the magnetometers by several orders of magnitude until $\gtrsim 400$ Hz. Power laws are observed over several ranges of k, consistent with turbulence. For $\sim 10^{-3}$ km$^{-1} < k < \rho_i^{-1}$, where the dynamics are expected to be governed by magnetohydrodynamics (MHD), the spectra scale as $\sim k^{-1.4}$. This power law is shallower than the $k^{-5/3}$ (Kolmogorov 1941) or $k^{-3/2}$ (Iroshnikov 1964; Kraichnan 1965) predictions from MHD. Surveys of magnetosheath turbulence show MHD-scale power laws have a broad distribution around $\sim k^{-1.2}$ with $k^{-5/3}$ occurring farther from the bow shock. This behavior may be due to fluctuations driven by the shock needing time to nonlinearly interact before the MHD-scale turbulence fully develops, producing a $k^{-5/3}$ spectrum (Huang et al. 2017). It is therefore reasonable to expect shallow power laws in the intervals analyzed here, due to the close proximity to the bow shock.
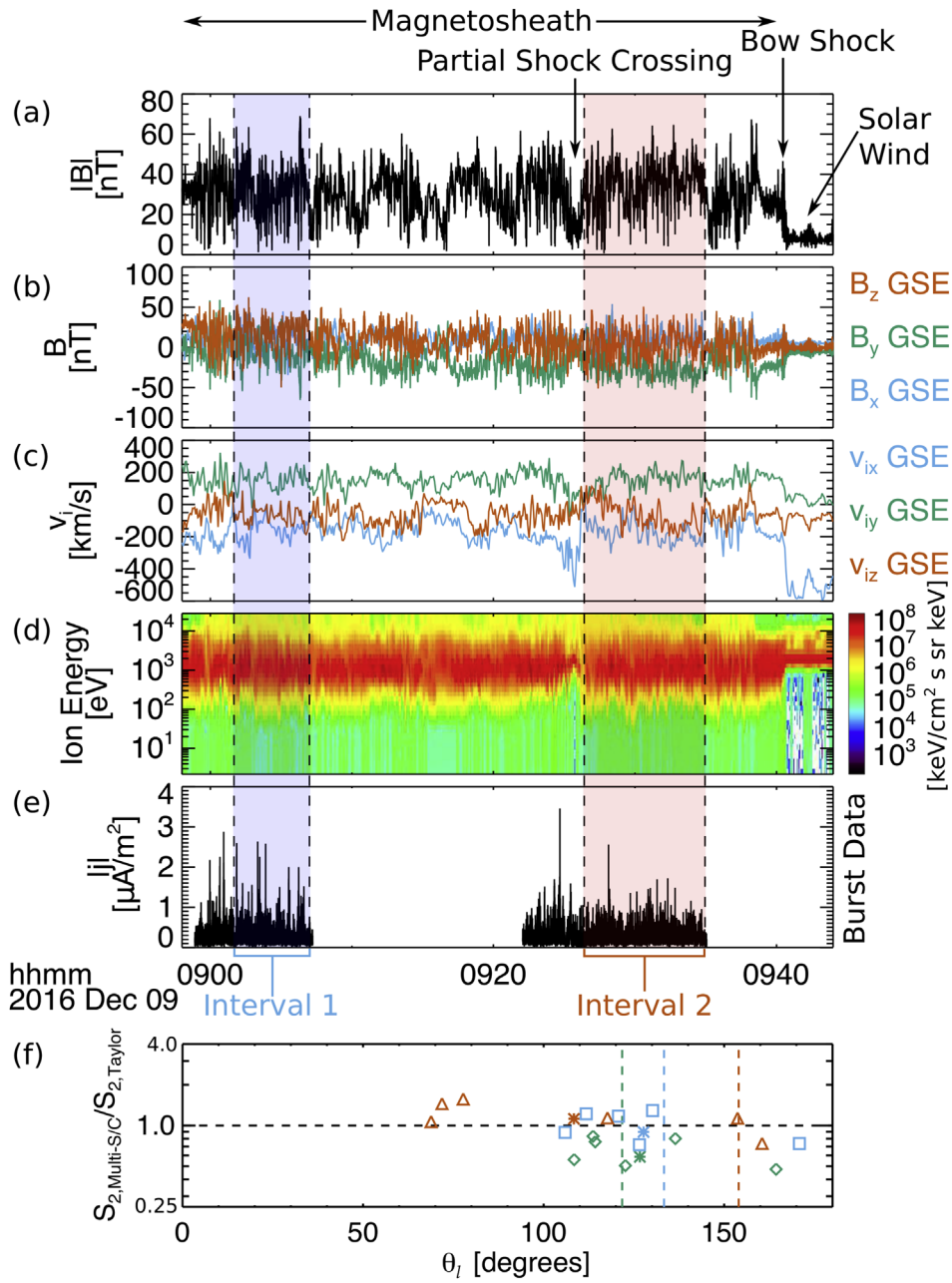
Figure 1. MMS1 observations, showing (a) $|\boldsymbol{B}|$, (b) $\boldsymbol{B}$ in GSE coordinates, (c) $\boldsymbol{v}_i$ in GSE coordinates, (d) ion energy spectrogram, and (e) $|\boldsymbol{j}|$ computed from FPI. $\boldsymbol{B}$ is plotted at 1/16 s cadence, particle data at 4.5 s cadence, and $|\boldsymbol{j}|$ at burst resolution. The analyzed intervals are shaded blue and red. (f) Ratio of multispacecraft to single-spacecraft estimates of S_2 as a function of θ_ℓ for Intervals 1 (blue squares) and 2 (red triangles) and the segment omitted from Interval 1 (green diamonds). The six points for each interval correspond to the six spacecraft pairs. Averages of the six points are marked with asterisks, and vertical dashed lines mark the $\boldsymbol{v}_0$ direction.

Table 1
Average Plasma and Fluctuation Properties

Interval	v_0 (km s^{-1})	v_A (km s^{-1})	$\delta b / B_0$	j_{rms} (μA m^{-2})	β_i	β_e	ρ_i (km)	d_i (km)	$\rho_e \sim d_e$ (km)	λ_c (d_i)
1	231	97	1.4	0.37	6	0.5	180	50	1	9–12
2	242	120	0.9	0.34	5	0.5	140	50	1	13

The spectra steepen to $\sim k^{-2.7}$ for Interval 1 and $\sim k^{-2.8}$ for Interval 2 at $k\rho_i \sim 1$. A spectral break at $k\rho_i \sim 1$ instead of $kd_i \sim 1$ agrees with solar wind observations (Chen et al. 2014) and simulations (Franci et al. 2016), showing the break tends toward ρ_i^{-1} for large β_i, as is the case here. The sub-ion-scale power laws match those observed at kinetic scales in the solar wind (Alexandrova et al. 2012), magnetosheath (Chen & Boldyrev 2017; Huang et al. 2017), and simulations (Franci et al. 2016, 2017), consistent with a turbulent environment. Recent simulations show fully developed kinetic-scale spectra can rapidly develop, facilitated by reconnection, even before a
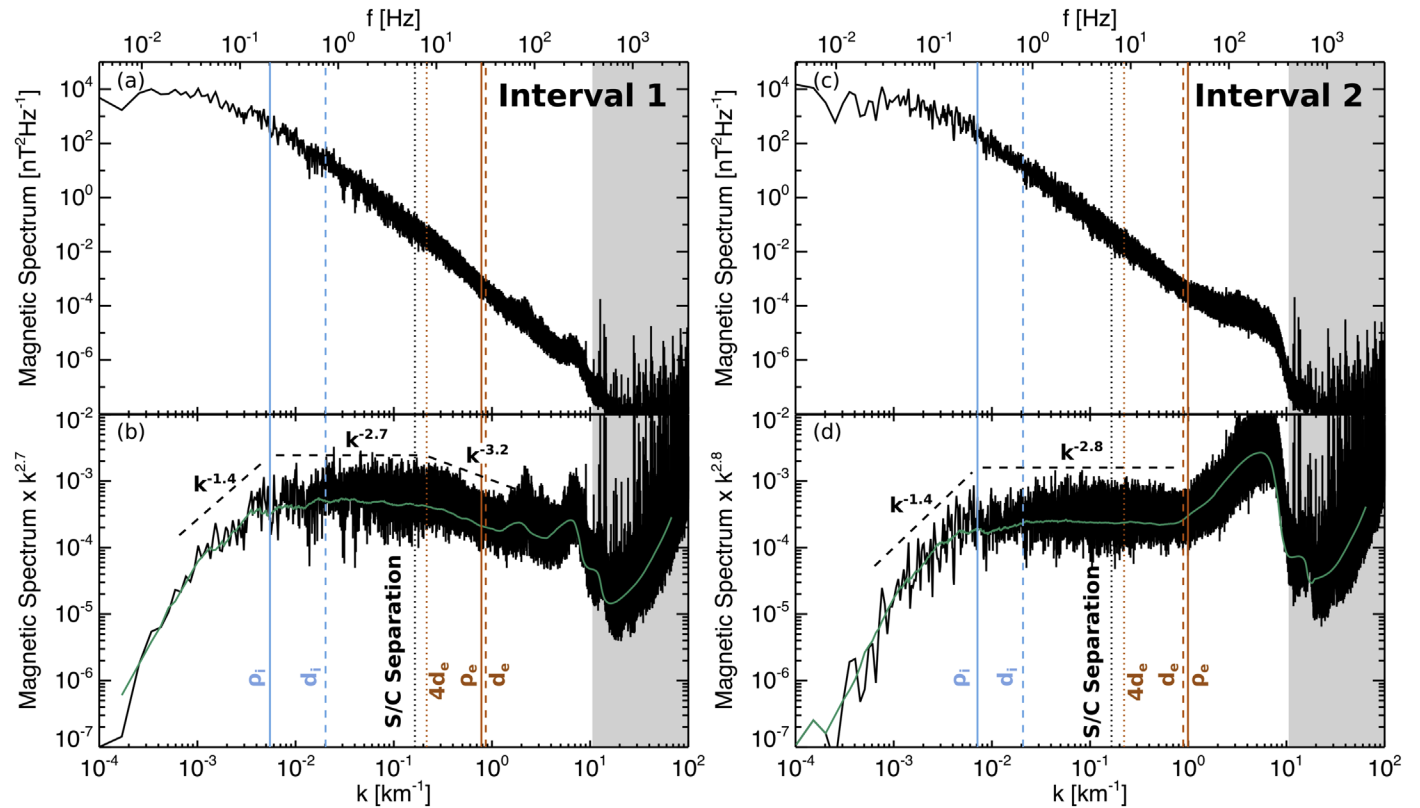
Figure 2. Omnidirectional magnetic spectra averaging together the four spacecraft for ((a)–(b)) Interval 1 and ((c)–(d)) Interval 2. The spectra from (a) and (c) are multiplied by the sub-ion-scale power law in (b) and (d), such that the spectra are constant just above $k\rho_i \sim 1$. Green curves are running medians over a half-decade in k. Vertical lines denote various inverse plasma length scales and the spacecraft separation. Shaded regions are where instrumental noise becomes significant.

fully developed MHD-scale inertial range forms (Franci et al. 2017).

The $k^{-2.8}$ scaling in Interval 2 continues to electron scales and an enhancement in magnetic power is present at sub-electron-scales, which may be related to wave activity. However, in Interval 1, a second steepening to $k^{-3.2}$ occurs at $k \sim (4d_e)^{-1}$. Interestingly, this length scale is similar to the thickness of the reconnecting current sheets identified by Phan et al. (2018), suggesting the steepening may be linked to reconnection. Such a steepening could either be due to dissipation, which may be facilitated by reconnection, or a change in the nonlinear dynamics. The disruption of current sheets by reconnection is suggested to alter the nonlinear dynamics at scales where the timescale of the tearing mode is faster than the nonlinear turbulence timescale, changing the spectral power law (Boldyrev & Loureiro 2017; Loureiro & Boldyrev 2017a, 2017b; Mallet et al. 2017). However, the theoretical description of this process is based on MHD turbulence models and new kinetic-scale models are needed to extend it to the electron reconnection observed here. Additionally, the thickness of intense current sheets is suggested to control the wavenumber of spectral breaks (Borovsky & Podesta 2015), which could produce the observed steepening if electron reconnection sets a thickness for the electron-scale current sheets.

While evidence of reconnection is found in both intervals, only Interval 1, which has the higher prevalence of reconnection, with 2.8 times as many reconnection events observed per unit time than Interval 2, shows a signature at $k \sim (4d_e)^{-1}$. As reconnection events occur at a subset of the current structures formed by the turbulence, one might expect the prevalence of

reconnection within a volume to impact how apparent the signature is in the spectrum. The prevalence of potential reconnection sites is explored further in the following section.

4.2. Current Distributions

To further examine conditions that may be favorable for reconnection within the two intervals, we examine the statistics of j, since large j could indicate thin current sheets. Both intervals have non-Gaussian distributions of each measurements of j for all three components, consistent with intermittency as expected in a turbulent plasma (Matthaeus et al. 2015), leading to nonexponential tails in the distribution of $|j|$ in Figure 3(a). However, the probability of the most intense currents ($|j| \gtrsim 2j_{\rm rms}$) is enhanced in Interval 1 relative to Interval 2. The higher probability of intense j in Interval 1 is also apparent in Figure 1(e) and indicates more potential reconnection sites may be present.

The distributions in Figure 3(a) depend upon the number of intense current structures and the dwell time within each structure. To verify the number of intense current structures, and thus the number of potential reconnection sites, is enhanced in Interval 1, we compute the cumulative distribution of peak currents ($j_{\rm peak}$) within each current structure in Figure 3(b). To identify current structures, local maxima in $|j|$ greater than $1.5j_{\rm rms}$ are identified, and two consecutive local maxima are considered independent structures if the local minimum between them is less than the half-maximum of either peak. Cumulative distributions are used instead of probability densities to avoid the need to set bin widths as there is a relatively small number of structures in each interval ($\sim$350
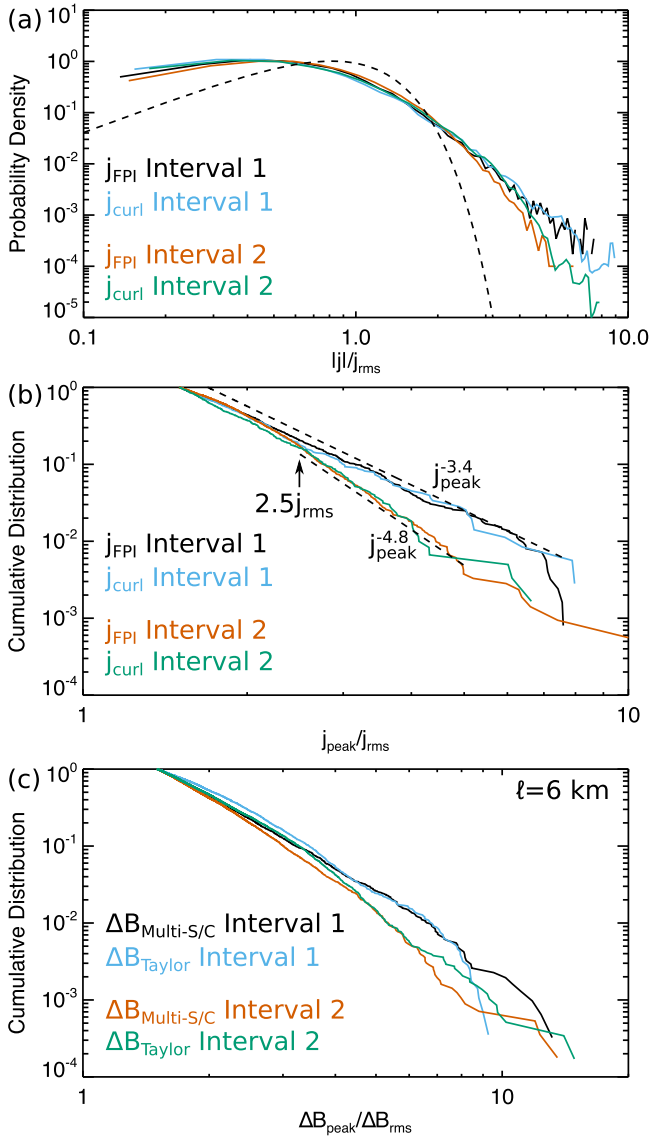
Figure 3. (a) Probability density of $|\boldsymbol{j}|$ with a dashed curve giving the distribution for the magnitude of a Gaussian random vector and (b) cumulative distributions of $j_{\text{peak}} > 1.5 j_{\text{rms}}$ computed from the curlometer and FPI moments. (c) Cumulative distribution functions of $\Delta B_{\text{peak}} > 1.5 \Delta B_{\text{rms}}$ for $\ell = 6$ km computed from multispacecraft increments and the Taylor hypothesis.

for Interval 1 and ~600 for Interval 2, consistent with the difference in length for the intervals). The identified current structures include the reconnecting current sheets identified by Phan et al. (2018). The cumulative distributions are similar, scaling as $j_{\text{peak}}^{-3.4}$, up to ~$2.5 j_{\text{rms}}$ for both intervals. Above $2.5 j_{\text{rms}}$, the cumulative distribution for Interval 2 steepens, while the distribution for Interval 1 maintains the same power law, indicating a lower prevalence of intense current structures in Interval 2.

Estimates of the half-maximum thickness for current sheets with $j_{\text{peak}} > 2.5 j_{\text{rms}}$ are < 130 km, indicating sub-ρ_i scale currents are more prevalent in Interval 1 than in Interval 2. Current sheet thicknesses are estimated by defining the normal direction ($\hat{\boldsymbol{n}}$) as $\hat{\boldsymbol{n}} \equiv \boldsymbol{B}_1 \times \boldsymbol{B}_2 / |\boldsymbol{B}_1 \times \boldsymbol{B}_2|$, where $\boldsymbol{B}_1$ and $\boldsymbol{B}_2$ are the magnetic field on either side of the current structure. The average $\boldsymbol{v}_i$ across the structure is used as the velocity.
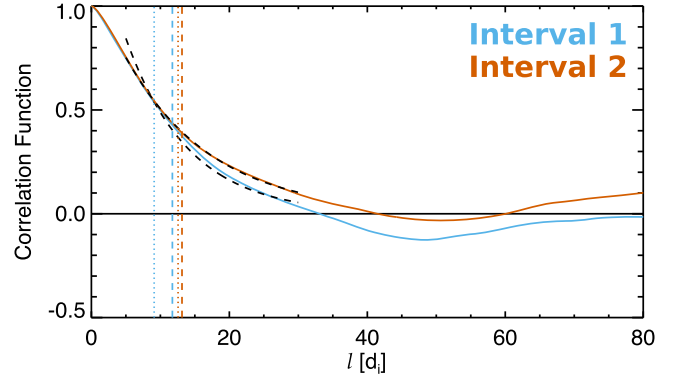

Figure 4. $R(\ell)$ computed from the Taylor hypothesis and averaging together the four spacecraft for Intervals 1 (blue) and 2 (red). Black dashed curves are exponential fits. Dashed and dotted vertical lines mark λ_c for each interval as computed from numerical integration and exponential fitting, respectively.

Cumulative distributions of the peak value for increments of $\boldsymbol{B}$ ($|\Delta \boldsymbol{B}(\ell)| \equiv |\boldsymbol{B}(\boldsymbol{x} + \ell) - \boldsymbol{B}(\boldsymbol{x})|$) in Figure 3(c) using multi-spacecraft measurements and the Taylor hypothesis are similar to those for $|\boldsymbol{j}|$. Therefore, the relative probability of intense structures in the increments can potentially be used to examine the prevalence of thin current sheets favorable for reconnection in turbulent plasmas where only single-spacecraft measurements and low-resolution plasma moments are available.

4.3. Correlation Length

While Section 4.2 gives insight into the prevalence of potential reconnection sites, we now examine why electron-only reconnection occurs in these intervals. The lack of ion jets within the reconnection events was suggested to be due to insufficient time and/or space for the ions to couple to the dynamics (Phan et al. 2018). Simulations of antiparallel reconnection suggest the MHD response to reconnection (including ion jets) weakens for current sheet lengths along the exhaust direction shorter than ~$10 d_i$ (Mandt et al. 1994). More recent guide field simulations with parameters comparable to Interval 1 find the MHD response weakens for lengths shorter than ~$40 d_i$, with little or no ion flows for lengths ~$10 d_i$ (Sharma Pyakurel et al. 2019). To asses this possibility, λ_c within the two intervals is examined. The autocorrelation function (R) of the magnetic fluctuations is given by

$$R(\ell) \equiv \frac{\langle \text{Tr} \left[\delta \boldsymbol{b}(\boldsymbol{x} + \ell) \delta \boldsymbol{b}(\boldsymbol{x}) \right] \rangle}{\langle |\delta \boldsymbol{b}|^2 \rangle}, \qquad (2)$$

where Tr[...] is the trace and $\delta \boldsymbol{b} \equiv \boldsymbol{B} - \langle \boldsymbol{B} \rangle$. $R(\ell)$ is estimated using the Taylor hypothesis and by averaging over time and the four spacecraft (Figure 4). The correlation length is estimated by numerical integration using $\lambda_c \equiv \int_0^\infty R(\ell) d\ell$, where the integration is performed up the first zero-crossing of $R(\ell)$, and by fitting an exponential of the form $R(\ell) \propto \exp(-\ell/\lambda_c)$.

For the two intervals, both methods for estimating λ_c give similar results. Estimates of λ_c are summarized in Table 1. MHD turbulence simulations show that the average length of reconnecting current sheets is ~λ_c (Servidio et al. 2009) and in Hall-MHD turbulence shorter and thinner reconnecting current sheets relative to MHD are present (Donato et al. 2012). The observed λ_c for the two intervals are ~$10 d_i$, consistent with the suggestion of Phan et al. (2018) that relatively short current sheets cause the lack of ion jets.

5

5. Conclusions

We examine two intervals of magnetosheath data where signatures of electron-only magnetic reconnection were identified at multiple electron-scale current sheets by Phan et al. (2018). We find that the fluctuations in these intervals have properties consistent with other turbulent plasmas, in that the magnetic spectrum at sub-proton scales is consistent with those commonly observed in the solar wind and numerical simulations. Both the currents and increments in the magnetic field have non-Gaussian statistics, consistent with intermittency. Magnetic spectra at scales larger than the ion gyroradius appear to have power laws shallower than those expected from turbulence theory, as often observed with magnetosheath turbulence. The correlation length of the turbulence is $\sim 10 d_i$, consistent with the current sheet length at which electron reconnection is expected to occur.

A new signature, where the magnetic spectrum steepens at $k > (4d_e)^{-1}$, is found in one of the intervals, which may suggest reconnection plays a role in dissipation at electron scales. While both intervals contain reconnecting current sheets, the spectral signature was found in the interval with more reconnection events, suggestive that such a steepening may become more apparent as more current sheets within the volume begin to reconnect. Additional theoretical work, focusing on electron-scale coherent structures, is needed to understand the link between the spectral break and reconnection.

Examining the distribution of current structures reveals that the interval with more reconnection events has an enhanced probability of intense sub-ion-scale current sheets, which may lead to more reconnection occurring. A clear change in the behavior of the cumulative distribution of $j_{\rm peak}$ at intense currents is present for the interval with reduced probability. Similar behavior is found in the distributions of magnetic increments, as often used to study turbulence, particularly when only single-spacecraft measurements are available.

This study highlights several new features that will be important to examine when studying reconnection in turbulent plasmas. At present, it is unclear why the two nearby intervals examined here exhibit these differences in the occurrence of intense small-scale current sheets and reconnection. One possibility may be the dynamical age of the turbulence. The interval with fewer reconnection events is observed immediately adjacent to a possible partial shock encounter, which suggests the turbulence was recently driven by processes at the shock. Depending on how far the other interval is from the shock, it may have had more time to develop nonlinearly and form intermittent current structures. However, it is not possible to confirm the distance of this interval from the shock with the present observations. Alternatively, the firehose instability can stabilize current sheets against reconnection and may influence kinetic-scale statistics (Matteini et al. 2013). Temperature anisotropies within the two intervals are similar and near unity, potentially inconsistent with this scenario; however, such instabilities would naturally drive the anisotropy back toward stability. A further statistical study of reconnection, current structures, and turbulence properties in the magnetosheath will help to elucidate this issue and further characterize the new spectral break near electron scales.

ORCID iDs

J. E. Stawarz ● https://orcid.org/0000-0002-5702-5802
J. P. Eastwood ● https://orcid.org/0000-0003-4733-8319
M. A. Shay ● https://orcid.org/0000-0003-1861-4767
D. J. Gershman ● https://orcid.org/0000-0003-1304-4769
C. T. Russell ● https://orcid.org/0000-0003-1639-8298
M. R. Argall ● https://orcid.org/0000-0001-6315-1613
L. Franci ● https://orcid.org/0000-0002-7419-0527

References

Alexandrova, O., Lacombe, C., & Mangeney, A. 2008, AnGeo, 26, 3585
Alexandrova, O., Lacombe, C., Mangeney, A., Grappin, R., & Maksimovic, M. 2012, ApJ, 760, 121
Argall, M. R., Fischer, D., Le Contel, O., et al. 2018, arXiv:1809.07388
Boldyrev, S., & Loureiro, N. F. 2017, ApJ, 844, 125
Borovsky, J. E., & Podesta, J. J. 2015, JGRA, 120, 9256
Bruno, R., & Carbone, V. 2013, LRSP, 10, 2
Burch, J. L., Moore, T. E., Torbert, R. B., & Giles, B. L. 2016a, SSRv, 199, 5
Burch, J. L., Torbert, R. B., Phan, T. D., et al. 2016b, Sci, 352, aaf2939
Carbone, V., Veltri, P., & Mangeney, A. 1990, PhFl, 2, 1487
Chandran, B. D. G., Li, B., Rogers, B. N., Quataert, E., & Germaschewski, K. 2010, ApJ, 720, 503
Chasapis, A., Matthaeus, W. H., Parashar, T. N., et al. 2018, ApJL, 856, L19
Chen, C. H. K., & Boldyrev, S. 2017, ApJ, 842, 122
Chen, C. H. K., Klein, K. G., & Howes, G. G. 2019, NatCo, 10, 740
Chen, C. H. K., Leung, L., Boldyrev, S., Maruca, B. A., & Bale, S. D. 2014, GeoRL, 41, 8081
Cranmer, S. R., Asgari-Targhi, M., Miralles, M. P., et al. 2015, RSPTA, 373, 20140148
Donato, S., Servidio, S., Dmitruk, P., et al. 2012, PhPl, 19, 092307
Franci, L., Cerri, S. S., Califano, F., et al. 2017, ApJL, 850, L16
Franci, L., Landi, S., Matteini, L., Verdini, A., & Hellinger, P. 2016, ApJ, 833, 91
Gingell, I., Schwartz, S. J., Eastwood, J. P., et al. 2019, GeoRL, 46, 1177
Gosling, J. T., Phan, T. D., Lin, R. P., & Szabo, A. 2007, GeoRL, 34, L15110
Huang, S. Y., Hadid, L. Z., Sahraoui, F., Yuan, Z. G., & Deng, X. H. 2017, ApJL, 836, L10
Huang, S. Y., Sahraoui, F., Deng, X. H., et al. 2014, ApJL, 789, L28
Iroshnikov, P. S. 1964, SvA, 7, 566
Kiyani, K. H., Osman, K. T., & Chapman, S. C. 2015, RSPTA, 373, 20140155
Kolmogorov, A. N. 1941, DoSSR, 30, 301
Kraichnan, R. H. 1965, PhFl, 8, 1385
Le Contel, O., Leroy, P., Roux, A., et al. 2016, SSRv, 199, 257
Loureiro, N. F., & Boldyrev, S. 2017a, PhRvL, 118, 245101
Loureiro, N. F., & Boldyrev, S. 2017b, ApJ, 850, 182
Mallet, A., Schekochihin, A. A., & Chandran, B. D. G. 2017, MNRAS, 468, 4862
Mandt, M. E., Denton, R. E., & Drake, J. F. 1994, GeoRL, 21, 73
Matteini, L., Landi, S., Velli, M., & Matthaeus, W. H. 2013, ApJ, 763, 142
Matthaeus, W. H., & Lamkin, S. L. 1986, PhFl, 29, 2513
Matthaeus, W. H., Wan, M., Servidio, S., et al. 2015, RSPTA, 373, 20140154
Phan, T. D., Eastwood, J. P., Shay, M. A., et al. 2018, Natur, 557, 202
Phan, T. D., Paschmann, G., Twitty, C., et al. 2007, GeoRL, 34, L14104
Pollock, C., Moore, T., Jacques, A., et al. 2016, SSRv, 199, 331
Retinò, A., Sundkvist, D., Vaivads, A., et al. 2007, NatPh, 3, 236
Russell, C. T., Anderson, B. J., Baumjohann, W., et al. 2016, SSRv, 199, 189
Sahraoui, F., Belmont, G., Pinçon, J., et al. 2004, AnGeo, 22, 2283
Schekochihin, A. A., Cowley, S. C., Dorland, W., et al. 2009, ApJS, 182, 310
Servidio, S., Matthaeus, W. H., Shay, M. A., Cassak, P. A., & Dmitruk, P. 2009, PhRvL, 102, 115003
Sharma Pyakurel, P., Shay, M. A., Phan, T. D., et al. 2019, PhPl, submitted (arXiv:1901.09484)

Stawarz, J. E., Ergun, R. E., & Goodrich, K. A. 2015, JGRA, 120, 1845
Sundkvist, D., Retinò, A., Vaivads, A., & Bale, S. D. 2007, PhRvL, 99, 025004
Vörös, Z., Yordanova, E., Varsani, A., et al. 2017, JGRA, 122, 11442
Wang, S., Chen, L.-J., Bessho, N., et al. 2019, GeoRL, 46, 562

Weygand, J. M., Kivelson, M. G., Khurana, K. K., et al. 2005, JGR, 110, A01205
Wilder, F. D., Ergun, R. E., Burch, J. L., et al. 2018, JGRA, 123, 6533
Yordanova, E., Vörös, Z., Varsani, A., et al. 2016, GeoRL, 43, 5969